Bioorganic Chemistry 114 (2021) 105154

Contents lists available at ScienceDirect

Bioorganic Chemistry

journal homepage: www.elsevier.com/locate/bioorg

Design, synthesis and bioactivity study of evodiamine derivatives as multifunctional agents for the treatment of hepatocellular carcinoma

Xiaohong Fan [b,1], Jiedan Deng [b,1], Tao Shi [b,*], Huaixiu Wen [c], Junfang Li [b], Ziyi Liang [d], Fang Lei [b], Dan Liu [b], Honghua Zhang [b], Yan Liang [b], Xiangyong Hao [e,*], Zhen Wang [a,b,d,*]

[a] School of Pharmaceutical Science, University of South China, Hengyang 421001, China
[b] School of Pharmacy, Lanzhou University, Lanzhou 730000, China
[c] Key Laboratory of Tibetan Medicine Research, Northwest Plateau Institute of Biology, Chinese Academy of Sciences, Xining 810001, China
[d] State Key Laboratory of Applied Organic Chemistry, College of Chemistry and Chemical Engineering, Lanzhou University, Lanzhou 730000, China
[e] Department of General Surgery, Gansu Provincial Hospital, Lanzhou 730000, China

ARTICLE INFO

Keywords:
Hepatocellular carcinoma
Topo I
Evodiamine
Cancer-associated fibroblasts (CAFs)

ABSTRACT

Topoisomerase has been found extremely high level of expression in hepatocellular carcinoma (HCC) and proven to promote the proliferation and survival of HCC. Cancer-associated fibroblasts (CAFs) as a kind of key reactive stromal cell that abundantly present in the microenvironment of HCC, could enhance the metastatic ability and drug resistance of HCC. Therefore, developing new drugs that address the above conundrums would be of the upmost significant in the fight against HCC. Evodiamine, as a multi-target natural product, has been found to exert various biological activities such as anti-cancer and anti-hepatic fibrosis via blocking topoisomerase, NF-κB, TGF-β/HGF, and Smad2/3. Inspired by these facts, 15 evodiamine derivatives were designed and synthesized for HCC treatment by simultaneously targeting Topo I and CAFs. Most of them displayed preferable anti-HCC activities on three HCC cell lines and low cytotoxicity on one normal hepatic cell. In particular, compound **8** showed the best inhibitory effect on HCC cell lines and a good inhibition on Topo I *in vitro*. Meanwhile, it also induced obvious G_2/M arrest and apoptosis, and significantly decreased the migration and invasion capacity of HCC cells. In addition, compound **8** down-regulated the expression of type I collagen in the activated HSC-T6 cells, and induced the apoptosis of activated HSC-T6 cells. *In vivo* studies demonstrated that compound **8** markedly decreased the volume and weight of tumor (TGI = 40.53%). *In vitro* and *in vivo* studies showed that its effects were superior to those of evodiamine. This preliminary attempt may provide a promising strategy for developing anti-HCC lead compounds taking effect through simultaneous inhibition on Topo I and CAFs.

1. Introduction

Primary liver cancer is one of the most aggressive and refractory malignancies, and ranks the sixth (4.7%) in morbidity and the third (8.2%) in mortality [1]. Hepatocellular carcinoma (HCC) is the predominant form of primary liver cancer, and carries commonly a poor prognosis [2]. Most HCC patients are usually diagnosed as the intermediate stage when symptoms start to appear, losing the opportunity for radical treatment and conservative treatment strategy is usually the most suitable option [3]. However, most of the traditional chemotherapy agents have a lower efficacy on HCC for a widely various reasons [4]. For one thing, most of the advanced stage HCC patients are accompanied by hepatic injury and cirrhosis resulting in the damage of liver function, which limits the use of some systemic chemotherapy drugs. For another thing, liver, as a crucial metabolic organ in the body, possesses a specific group of cytochromes *P*-450 enzymes, which convert most drugs to metabolites or inactive forms leading to the chemotherapy resistance. Besides, the presence of a inflammatory and fibrotic

Abbreviations: TGF-β, transforming growth factor-β; Topo I, topoisomerase I; Topo II, topoisomerase II; HSC, hepatic stellate cell; EVO, Evodiamine; TME, tumor microenvironment; HCC, Hepatocellular carcinoma; CAFs, Cancer-associated fibroblasts; Col-1, type I collagen; FBS, fetal bovine serum; m, multiplet (spectral); IC_{50}, half-maximum inhibitory concentration; i.p., Intraperitoneal injection; HE, Hematoxylin and eosin stain; DMSO, dimethyl sulphoxide; SD, standard deviation; SEM, standard error of mean; PBS, Phosphate-buffered saline.

* Corresponding authors at: School of Pharmaceutical Science, University of South China, Hengyang 421001, China (Z. Wang).
E-mail addresses: shit18@lzu.edu.cn (T. Shi), haoxy-2008@163.com (X. Hao), zhenw@lzu.edu.cn (Z. Wang).
[1] These authors made equal contributions to this work.

https://doi.org/10.1016/j.bioorg.2021.105154
Received 2 March 2021; Received in revised form 16 June 2021; Accepted 4 July 2021
Available online 7 July 2021

microenvironment in HCC could induce chemotherapy resistance by releasing cytokines and extracellular matrix [5]. Based on the above considerations, fewer choices exist for systemic chemotherapy on advanced HCC [6]. Sorafenib as an anti-angiogenic and anti-proliferation drug is the only first-line systemic therapy agent for advanced HCC [7]. Whereas, it minimally provides survival improvements, and thus developing more effective therapeutic strategies for advanced HCC is urgently needed.

According to the references, on the one hand, topoisomerase I and II (Topo I and II) genes are highly expressed in the HCC tissue, and correlate positively with the occurrence and development of HCC [8]. Numerous Topo inhibitors, including topotecan, irinotecan and doxorubicin, are now widely used in the clinical setting. However, they have limited efficacy in hepatocellular cancer, and one of the main reasons for this is underlying chemoresistance in HCC microenvironment. On the other hand, 90% of HCC cases always occur in the setting of cirrhosis and chronic liver diseases,[9] and the fibrotic microenvironment plays an important role in the occurrence, metastasis and chemoresistance of HCC [4,10]. In addition, multiple interactive processes among heterogeneous cell types are extremely complex and could influence HCC progression [11–12]. Among them, cancer-associated fibroblasts (CAFs) as a key and abundant type of stromal cells which are thought to probably derive from activated hepatic stellate cells (HSCs), could provide a favorable setting by secreting various immunosuppressive and cancer-supportive soluble factors into the microenvironment [13]. These secreted components could promote multiple aspects of HCC progression and growth by remodeling the TME in favor of cancer expansion and therapeutic resistance [14]. Therefore, developing multi-functional drugs holds a promise for combating this highly lethal cancer.

Natural products are an important source of therapeutic drugs [15]. More than half of cancer chemotherapeutic drugs come from natural products and their derivatives [15]. Evodiamine (EVO), an indolequinone alkaloid extracted from Evodia, is a new promising natural anti-cancer lead compound against a broad spectrum of cancers by dual inhibition on topoisomerase I and II (Topo I and II) proteins which have long been considered as one of the most effective chemotherapeutic targets [8,16–17]. Notably, some reports have indicated that EVO could significantly reverse the CAFs phenotype and remodel tumor microenvironment (TME) via blocking the Smad 2/3 signaling pathway [18]. Moreover, it also exerts a favorable anti-hepatic fibrosis activity *via* inhibiting TGF-1β/Smad pathway [19–20]. In view of its multi-target and broad-spectrum anti-cancer activities as well as the potency of remodeling TME, EVO could be regarded as an excellent anti-HCC candidate. Unfortunately, previous studies have stated that EVO possesses lower inhibitory activity on Topo I/II and is easily transformed into inactive metabolites in the liver [21–23]. These characteristics of EVO may cause unsatisfactory *in vivo* anticancer activity and sorely limits its further application in HCC treatment [22,24]. Therefore, many excellent researches aim for improve its anticancer efficacy and reduce its toxicity through various molecular modeling and drug design techniques [25–29]. Admirably, Sheng and co-workers [25,27–28,30] has done pioneering works in the development of novel agents based on evodiamine.

In view of the above-mentioned points, firstly, topoisomerase inhibitors, a class of broad-spectrum chemotherapy agents, yet in fact they have limited efficacy in hepatocellular cancer and one of the main reasons for this is underlying chemoresistance in HCC microenvironment. Development of highly potential and multi-functional topoisomerase inhibitors that address this critical challenge would therefore be of the most importance in the fight against HCC. Secondly, EVO, as a multi-target natural molecule, possesses anti-cancer activity and modulation of inflammatory and fibrotic microenvironment (Scheme 1), and it has the potential to be developed into anti-HCC agents with higher efficient and lower toxic. Thirdly, EVO possesses unsatisfactory inhibitions on Topo I/II and is easily transformed into extensive metabolism in the liver, among them, *N*-demethylation metabolic pathways will lead to inactivity [28,31]. We hypothesized that replacing methyl group in N14 position with more bigger groups or introducing various isosteres may improve the anti-HCC efficiency of EVO (Scheme 1). To achieve these goals, we rationally designed and synthesized a series of EVO derivatives (Scheme 2) based on our previously reported synthetic processes [32]. In this protocol, we were able to modify different atoms or substituents on the original N14 position to improve anti-cancer potency. Inhibiting Topo I and reducing CAFs activation to show excellent anti-liver cancer efficiency *in vitro* and *in vivo* was proven by the subsequent structure–activity relationships study (SARs) and biological evaluation. This study may provide a guidance for further optimizing the structure of evodiamine and developing multi-functional anti-HCC agents.

2. Results and discussion

2.1. Chemistry

To explain and predict the SARs of EVO, 15 compounds were synthesized by the one-step construction of three chemical bonds and two heterocyclic-fused rings according to our previously reported method [32]. The purity of all compounds was monitored by HPLC and was>95.0%, which established solid foundation for the further biology

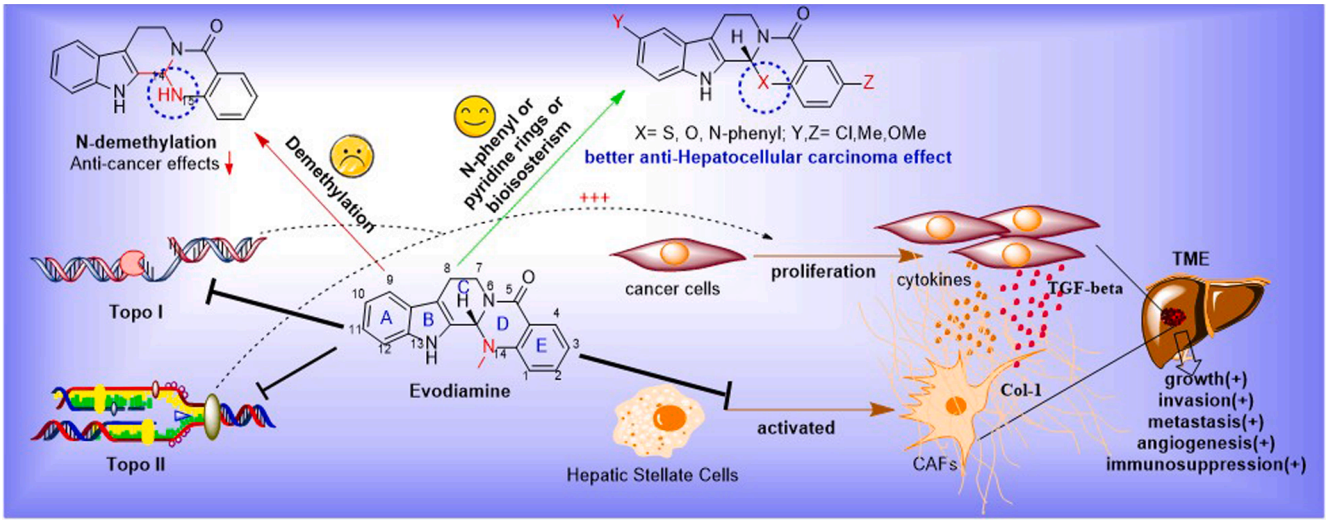

Scheme 1. Rational design of evodiamine derivatives and its anti-HCC mechanism.

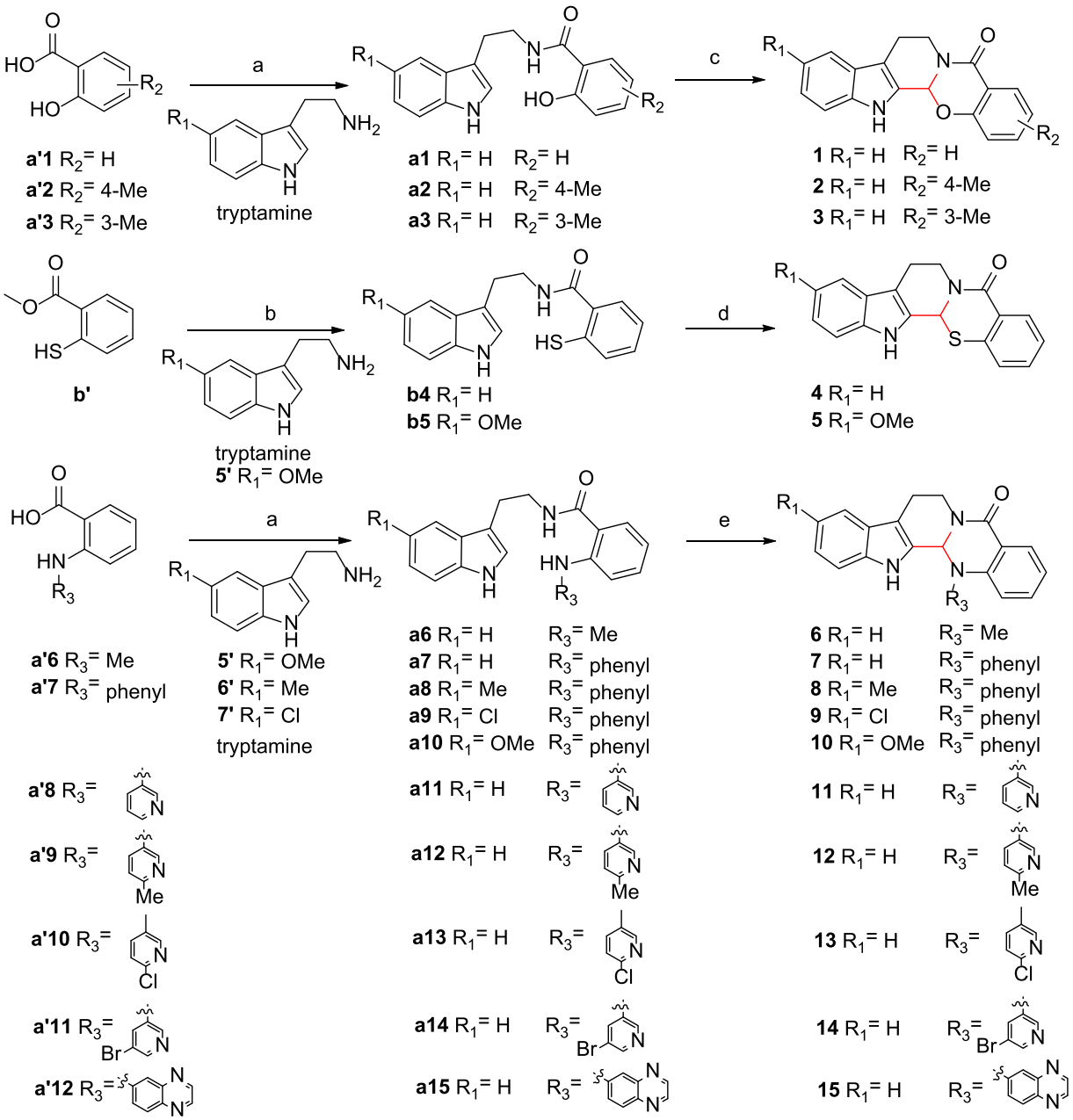

Scheme 2. Synthetic route to evodiamine derivatives. (a) EDCI, HOBt, TEA, DCM, r.t., 16 h; (b) $AlMe_3$, DCM, r.t., 8 h; (c) $HC(OEt)_3$, $BF_3{\cdot}Et_2O$, DMF, 135 °C; (d) $HC(OEt)_3$, $BF_3{\cdot}Et_2O$, DCM, r.t; (e) $HC(OEt)_3$, $BF_3{\cdot}Et_2O$, DMF, 100 °C.

activity exploration. Compounds **1** [32], **2** [27], **3** [27], **4** [32–33], **5** [32], **6** [32], **7** [32], **8** [32], **9** [32], **10** [32] have been reported previously, while compounds **11** to **15** are new.

2.2. Biology

2.2.1. In vitro Anti-proliferation activity and SARs

The anti-proliferation activity of all compounds against human normal liver cell line (HL-7702) and HCC cell lines (HepG2, MHCC-LM9, Huh-7) were evaluated by Cell Counting Kit-8 (CCK-8) assay, with evodiamine as the parent compound and Sorafenib as the positive control. As shown in Table 1, the toxicity of evodiamine derivatives on normal human liver cells HL-7702 was lower than evodiamine and sorafenib, and the IC_{50} values of synthesized compounds were higher than 40 μM, except for compound **1** (37.75 ± 4.72 μM). In the oxo-evodiamine derivatives (compounds **1**–**3**), replacing nitrogen atom on the 14 position of EVO with oxygen atom would decrease the anti-proliferation activity on MHCC-LM9 and Huh7 cells. Introducing methyl group in R_2-4 position, the anti-proliferation activity dramatically decreased (compound **2**), and introducing methyl group in R_2-3 position, the anti-proliferation activity slightly increased (compound **3**) on three HCC cell lines. In the thio-evodiamine derivatives (compounds **4** and **5**), an increasing trend of activity was observed on HepG2 and Huh7 cells, and introducing methoxy group in 10 position (compound **5**) showed lower activity against MHCC-LM9 cells than compound **4**. In the *N*-phenyl-derivatives, the inhibition order was **8 > 9 > 7 > 10** on MHCC-LM9 and Huh7 cells. The anti-proliferation activity of the compounds substituted with methoxy decreased slightly, but the activity on HepG2 cell line enhanced. Besides, the replacement of phenyl rings by pyridine rings and quinoxaline ring caused reduction of anti-proliferative activity (compounds **11** and **15**, IC_{50} > 40 μM). In general, *N*-phenyl and sulfur atom substitutions on 14 position were more active than oxygen atom

Table 1
Anti-proliferation activity of compounds on different liver cell lines.

Compd.	$IC_{50} \pm SD$[a] (μM)			
	MHCC-LM9	Huh7	HepG2	HL-7702
1	37.71 ± 0.47	9.92 ± 0.66	21.10 ± 1.53	37.75 ± 4.72
2	>40	>40	>40	>40
3	10.21 ± 1.07	1.06 ± 0.28	10.06 ± 3.12	>40
4	0.34 ± 0.10	0.28 ± 0.05	2.30 ± 0.23	>40
5	3.76 ± 1.18	0.65 ± 0.12	2.45 ± 0.38	>40
6(EVO)	1.63 ± 0.28	0.78 ± 0.22	21.52 ± 2.14	26.32 ± 5.45
7	9.82 ± 2.13	0.74 ± 0.10	2.39 ± 0.45	>40
8	0.24 ± 0.05	0.44 ± 0.12	0.92 ± 0.20	>40
9	0.53 ± 0.01	0.72 ± 0.28	1.11 ± 0.27	>40
10	>40	4.86 ± 0.56	0.54 ± 0.16	>40
11	>40	>40	>40	>40
12	>40	>40	>40	>40
13	>40	>40	>40	>40
14	>40	>40	>40	>40
15	>40	>40	>40	>40
Sorafenib	7.74 ± 0.80	10.12 ± 0.03	5.58 ± 0.46	5.61 ± 0.58

[a] CCK-8 assay; cells exposed to tested compounds at the concentrations of 0, 0.156, 0.625, 2.5, 10, 40 μM for 48 h; the data were presented as mean ± SD ($n \geq 3$).

substitutions for HCC cell lines. Finally, the substitution of different atoms on 10 position has a certain effect on the activity.

Although different compounds displayed various activity against diverse tested cell lines. Fortunately, compounds **4** and **8** displayed extremely preferable anti-proliferation on three HCC cells and they were less toxic to normal liver cells than both sorafenib and evodiamine. Therefore, compounds **4** and **8** were selected for Topo I inhibition assay.

2.2.2. *Topo I inhibitory effect of compounds 4 and 8*

According to the report, evodiamine has been proven to be an inhibitor of Topo I/II [17], therefore, target verification experiments of the selected compounds **4** and **8** on Topo I were carried out. The results were shown in Fig. 1. Topo I-mediated relaxation of supercoiled DNA was significantly inhibited by compounds **8** and **4** at a concentration of 100 μM, while evodiamine showed no inhibitory activity at the same concentration. Then, as the concentration gradiently decreased from 100 to 10 μM, the inhibitory activity of compounds **8** and **4** on Topo I also significantly weakened, while camptothecin (CPT) still had strong inhibitory activity at the lowest concentration of 10 μM. At a concentration of 50 μM, compound **8** still retained potent inhibitory activity, but compound **4** showed no inhibitory activity. These results demonstrated that compounds **8** and **4** could inhibit Topo I and the activity of compound **8** is a little better than that of compound **4**. Therefore, we chose compound **8** for the following anti-tumor experiments *in vitro* and *in vivo*.

2.2.3. *Anti-proliferative effect of compound 8 on MHCC- LM9 and Huh7 Cells*

To further verify the anti-proliferative effect of compound **8**, EdU and colony formation assay were employed to more accurately observe the cell proliferation of MHCC-LM9 and Huh7 cells treated by compound **8** and EVO (0.1, 0.3, 0.9 μM). As shown in the Figs. 2 and 3, both compound **8** and EVO exerted markedly antiproliferative activity in MHCC- LM9 and Huh7 cells and the inhibitory activity of compound **8** at tested concentrations was superior to that of evodiamine in both experiments. To our delight, the relative colony formation ratios in MHCC-LM9 of compound **8** at the 0.1, 0.3, 0.9 μM<10%, thus confirmed its outstanding antiproliferative capacities.

2.2.4. *Compound 8 induced cell cycle G_2/M arrest in Huh7 and MHCC-LM9 cells*

To confirm the effect of compound **8** on cell cycle progression in Huh7 cells and MHCC- LM9 cells, the flow cytometric assay was performed. The cell cycle distribution in Huh7 cells and MHCC- LM9 were detected after a 48 h-exposure to compound **8** and EVO at different concentrations. As shown in Fig. 4, the G_2/M phase arrests were significantly in a trend of dose-dependent change and compound **8** showed remarkably better activity than EVO. During the process of increasing the concentration of compound **8** from 0.1 μM to 0.9 μM, the proportion of G_2/M phase in MHCC-LM9 and Huh7 cells increased from 25.53% to 78.75% and 20.87% to 63.32%, respectively. In contrast, the ratios of untreated Huh7 and MHCC- LM9 cells in G_2/M cell cycle were 13.86% and 23.21%, respectively, which were lower than those in the compound **8** group. After incubating with EVO at 0.1, 0.3 and 0.9 μM, the proportion of G_2/M phase in MHCC-LM9 and Huh7 cells were changed gently (16.97% to 44.34% and 19.37% to 46.81%, respectively). The cell cycle G_2/M arrest of compound **8** at tested concentrations still was superior to that of EVO.

2.2.5. *Compound 8 promoted cell apoptosis on Huh7 cells*

Anti-cancer activity of Topo inhibitors is often related with induced cell apoptosis [34]. To further assess the anti-HCC effect of compound **8**, firstly Giemsa staining assay was performed on Huh7 cells by treating the cells with compound **8** at gradient concentrations (0.15, 0.3, 0.6 μM) for 24 h. As depicted in Fig. 5**A**, cells treated with compound **8** showed classic apoptosis (marked by green arrows), such as cell swelling, karyopyknotic, nuclear fragmentation or agglutination, and apoptotic body formation compared to the normal cells. To further confirm the apoptosis effects of compound **8**, flow cytometry analysis was performed. The apoptosis of cells exposed to compound **8** and EVO at different concentrations after 48 h, stained with Annexin V-FITC and PI. As showed in Fig. 5**B**, the number of late apoptotic cells in the compound **8** and **EVO** treatment groups were remarkably increased from 29.4% to

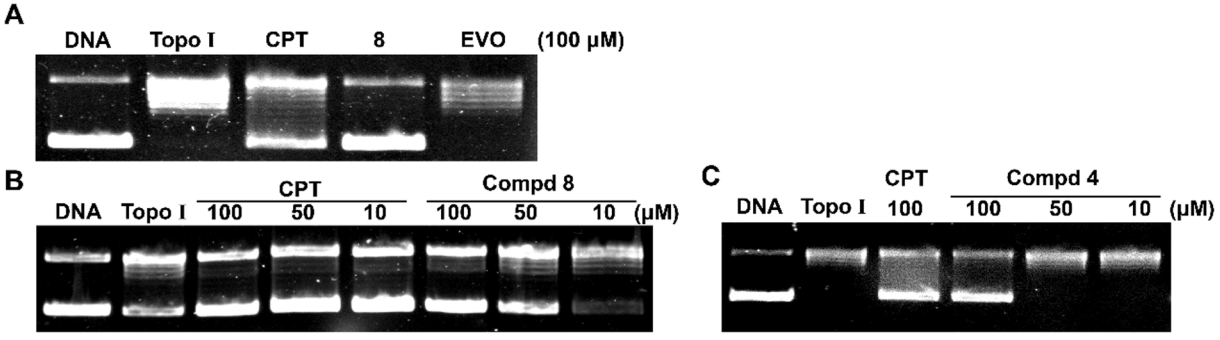

Fig. 1. Topo I inhibitory activity of compounds **8** and **4 (A)** Inhibition activity on Topo I relaxation at 100 μM. Lane 1, supercoiled plasmid DNA; lane 2, DNA + Topo I; lane 3, DNA + Topo I + CPT; lane 4, DNA + Topo I + compound **8**; lane 5, DNA + Topo I + EVO. **(B)** Inhibition on Topo I relaxation at different concentrations: lane 1, supercoiled plasmid DNA; lane 2, DNA + Topo I; lanes 3–5, DNA + Topo I + CPT (100, 50 and 10 μM); lanes 6–8, DNA + Topo I + compound **8** (100, 50 and 10 μM). **(C)** Topo I inhibitory activity of compound **4**. Lane 1, supercoiled plasmid DNA; lane 2, DNA + Topo I; lane 3, DNA + Topo I + CPT; lanes 4–6, DNA + Topo I + compound **4** (100, 50 and 10 μM).

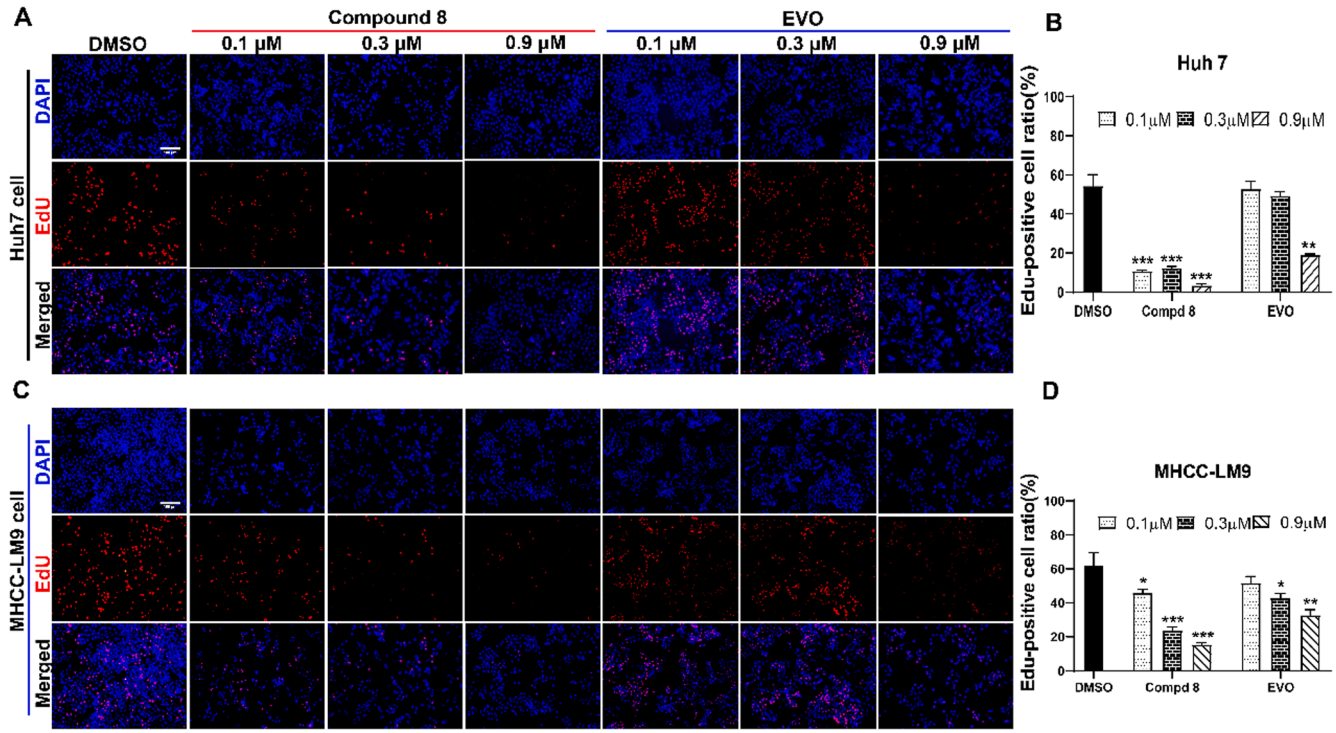

Fig. 2. Compound **8** weakened markedly antiproliferative activities in Huh7 and MHCC-LM9 cells detected by EdU (red) staining. MHCC-LM9 and Huh7 cells exposed to EVO and compound **8** at different concentrations for 24 h before EdU staining. Images showed representative pictures of inhibitions of compound EVO and compound **8** on Huh7 (A) and MHCC-LM9 (C) cells proliferation were determined by EdU proliferation assays (magnification × 10, scale bar = 100 μm). The statistical data of the EdU-positive cell ratio to DMSO groups in Huh7 (B) and MHCC-LM9 cells (D). Data are presented as mean ± SD from three independent experiments. *P < 0.05; **P < 0.01, ***P < 0.001 compared with the DMSO group. (For interpretation of the references to colour in this figure legend, the reader is referred to the web version of this article.)

40.3% and 14.8% to 28.0%, respectively. Induced apoptosis activity of compound **8** at tested concentrations was more effective than EVO treatment. These results demonstrate that compound **8** effectively induces the apoptosis of Huh7 cells.

2.2.6. Compound 8 reduced the invasion and migration activity of MHCC-LM9 and Huh7 cells

The migration and invasion of cancer cells can explain their malignancy to some extent. It has been reported that Topo I/II inhibitors could down-regulate MMP9 mRNA to reduce the invasion ability of cells and further alleviate cancer metastasis [35]. Some researches has shown that EVO could suppress the invasion, migration and VEGF-induced angiogenesis of HCC *in vitro* and *vivo* via reducing the expression of β-catenin and VEGF [36]. Herein, to explore the effect of compound **8** on the invasion and migration of MHCC-LM9 and Huh7 cells, the chamber transwell and scratch assay were employed. In the transwell assay, as shown in Fig. 6**,** MHCC-LM9 had a weak invasion and migration ability for 24 h, compared to Huh7 cells. To our delight, compound **8** dose-dependently obvious inhibited the migration and invasion of both HCC cell lines. In the scratch wound healing assay, the horizontal migration distance of MHCC-LM9 and Huh7 cells that were exposed to compound **8** and EVO were significantly reduced compared with the control cells (Fig. 7). Similarly, compound **8** performed better than EVO in both assays.

2.2.7. Compound 8 inhibited the activation of HSC-T6 cells, inhibited the proliferation and induced the apoptosis of activated HSC-T6 cells

Hepatic stellate cell (HSC), also known as lipid storage cells, is mainly located in the space around the hepatic sinus, accounting for 5% ~23% of hepatic stromal cells [12]. Normally, HSC had low proliferative activity and weak ability to synthesize collagen [37]. When HSC is stimulated by various physical and chemical factors and viral infection, it can be activated, and the activated HSC will transform into contractive and highly proliferative myofibroblast-like cells, and produce a large amount of extracellular matrix, leading to liver fibrosis, and then to cirrhosis, and ultimately to liver cancer [38]. It is the main source of Cancer-associated fibroblasts (CAFs), involved in the tumor microenvironment with diverse functions, including remodeling and matrix deposition, interacting closely with cancer cells and crosstalk with other stromal cells [38–39]. Some evidences show that hepatic stellate cells secrete type I collagen (Col-1) to promote the invasion and metastasis ability of hepatoma cells by induction of the epithelial-mesenchymal transition (EMT) [40]. Therefore, CAFs have become a potential target for optimizing therapeutic strategies against HCC. To investigate the effect of compound **8** on CAFs, HSC-T6 cell lines were exposed to the compound **8** and EVO at concentrations of 0.1, 0.3 and 0.9 μM for 24 h in the presence of TGF-β (10 ng/mL) to induce HSC-T6 cells activating. The Col-1 level of HSC-T6 cells was determined by ELISA assay after treatment for 24 h. As illustrated in Fig. 8 **A,** the Col-1 level of activated HSC-T6 cell increased significantly after being stimulated by TGF-β (10 ng/mL). But after compound **8** and EVO treatment at gradient concentrations (0.1, 0.3, 0.9 μM) for 24 h, the Col-1 level significantly reduced, indicating that compound **8** and EVO could suppress the activation of HSC. In order to further explore the effect of compound **8** on apoptosis and proliferation of activated HSC-T6, firstly, cells were stimulated by TGF-1β (10 ng/mL) for 24 h, and then cells were treated with compound **8** and EVO at concentrations of 0.1, 0.3 and 0.9 μM for 24 h. The results are shown in Fig. 8 **B** and **C,** indicating that compound **8** and EVO markedly suppressed proliferation and induced apoptosis of activated HSC-T6 cells, and EVO displayed lower activity than compound **8.**

2.3. Compound 8 inhibited MHCC-LM9 tumor xenograft growth in vivo

Based on significant anti-HCC activity of compound **8** in vitro, the

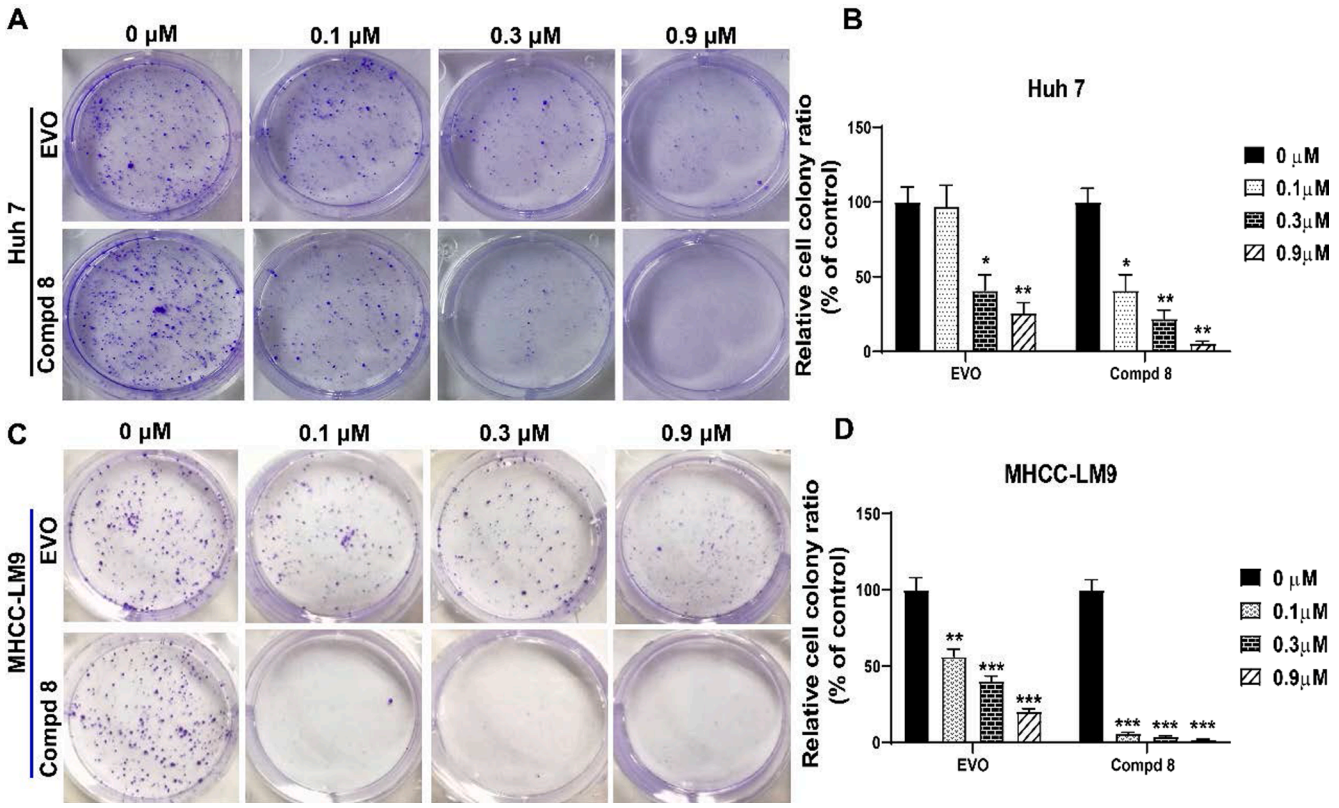

Fig. 3. Compound **8** decreased colony formation of Huh7 and MHCC-LM9 cells. Huh7 cells seeded at low density and exposed to EVO and compound **8** (0.1, 0.3 and 0.9 μmol/L) for 14 d. Representative images of plate clone formation assays of Huh 7 (A) and MHCC-LM9 cells (C) stained by 1% crystal violet. The statistical data of the relative cell colony ratio to control groups (0 μM) in Huh 7 (B) and MHCC-LM9 cells (D). All statistical data are presented as the mean ± SD of three experiments. *P < 0.05; **P < 0.01, ***P < 0.001 compared with the control group. (For interpretation of the references to colour in this figure legend, the reader is referred to the web version of this article.)

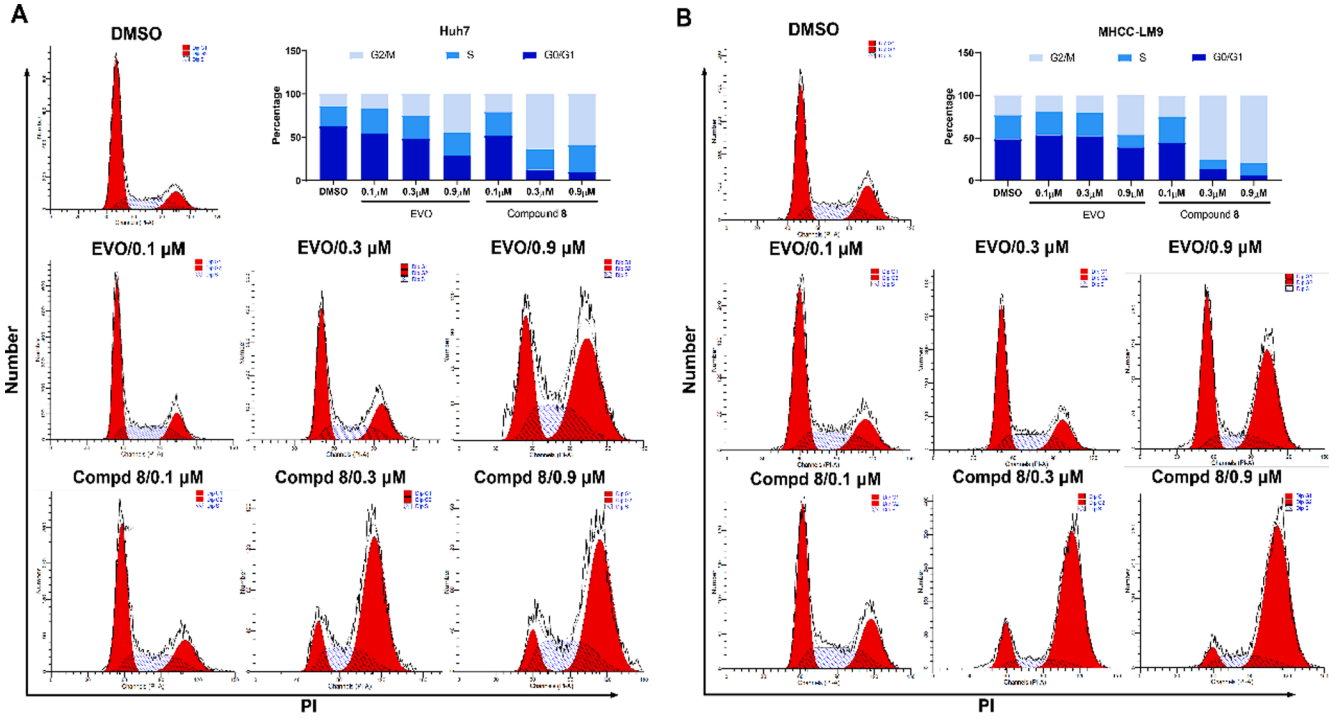

Fig. 4. Compound **8** caused cell cycle G_2/M arrest in Huh7 and MHCC-LM9 cells. Flow cytometric analysis of DNA tested using PI staining after exposed to EVO and compound **8** (0.1, 0.3, 0.9 μM) for 48 h in Huh7(A) and MHCC-LM9 (B). The illustration in the upper right corner represented percentage of each cell phase.

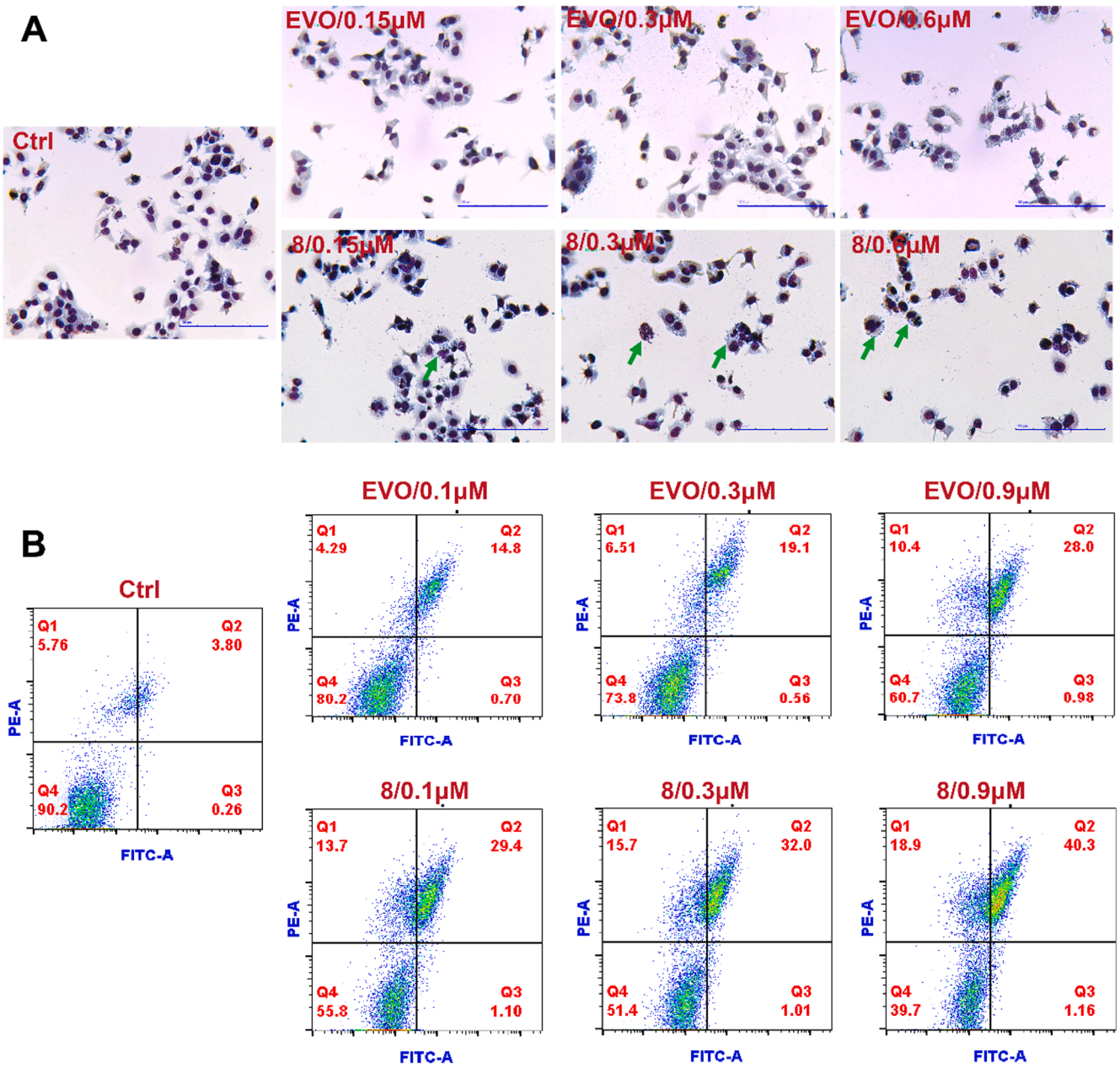

Fig. 5. Compound **8** changed morphology and induced apoptosis of Huh7 cells. Cell morphological changes of Huh7 cells stimulated by the treatment of compound **8** and EVO at gradient concentrations (0.15, 0.3, 0.6 μM) for 24 h and stained by Giemsa reagents and detected by microscopy (magnification 200×, scale bar = 500 μm). Green arrows point apoptotic cells characterized by cell swelling, karyopyknotic, nuclear fragmentation or agglutination, and apoptotic body formation (A). Apoptosis analysis of Huh7 cells induced by compound **8** and EVO using flow cytometric after cells stained by Annexin V/PI double staining (B). (For interpretation of the references to colour in this figure legend, the reader is referred to the web version of this article.)

preliminary efficacy experiments on the MHCC-LM9 tumor xenograft model in mice was prepared. MHCC-LM9 cells were injected into the subcutaneous right forelimb armpit. Mice were randomly divided into four groups after the tumors had grown to an average size of about 100 mm^3. Sorafenib at the dose of 10 mg/kg as the positive control (twice a day, intraperitoneal injection), Compound **8** and EVO at the dose of 50 mg/kg were injected intraperitoneally for 3 weeks (twice a day). As shown in the Fig. 9, compound **8** obviously inhibited tumor growth and decreased the weight and volume of tumor with a tumor growth inhibition rate of 40.53%. More importantly, the body weight of mice in treatment groups had no significant difference compared to control group. Besides, the anti-tumor activity of the sorafenib was better even at a lower dose, while that of the compound **8** was improved to a certain extent compared with that of EVO. Subsequently, the tumor tissue was harvested for hematoxylin and eosin stain (HE) staining. The results displayed that high density of new blood vessels was observed in the control group and EVO treatment group (highlighted by black arrows) (Fig. 10). By contrast, compound **8** administration treatment reduced formation of new blood vessels and did not show any significant changes in the heart, lung, liver, kidney or spleen (Fig. 10). In addition, no significant change was observed in simple routine blood test and blood biochemistry between compound **8** group and control group (**Table S1 and S2**).

3. Conclusion

Hepatocellular carcinoma (HCC) is an intractable malignant cancer that usually occurs in the setting of chronic liver inflammation and

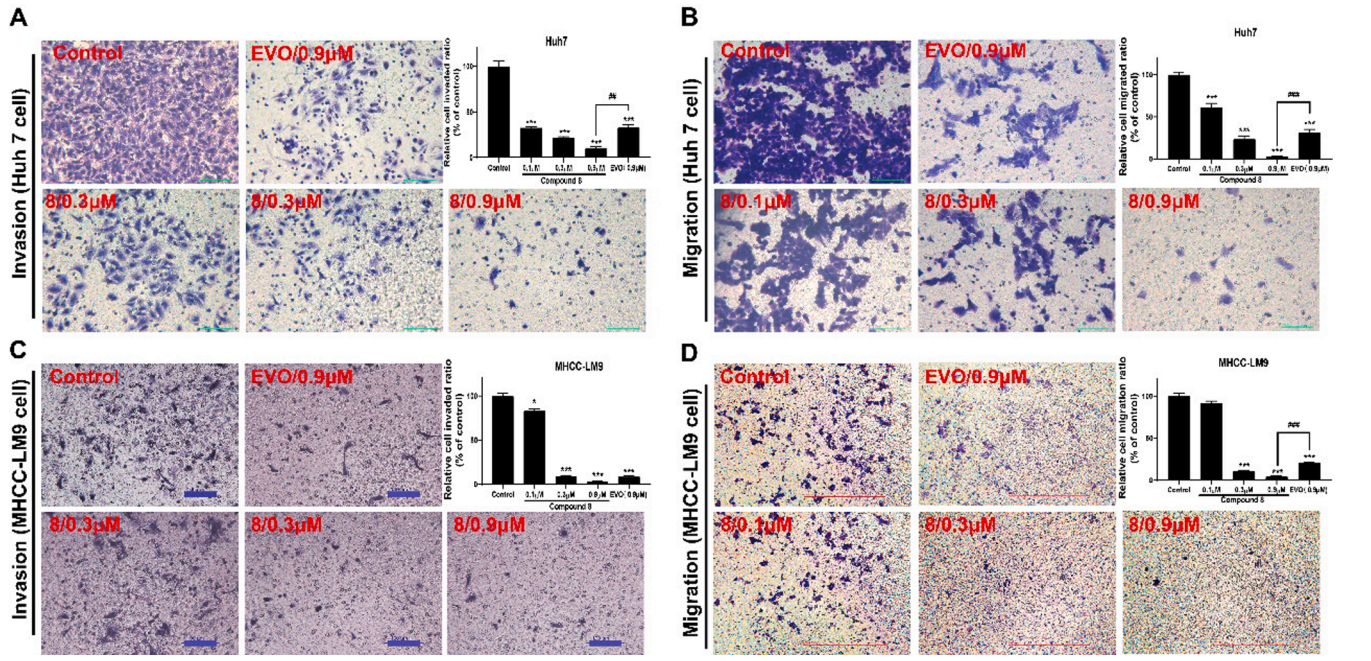

Fig. 6. Compound **8** attenuated migration and invasion capacities of Huh7 and MHCC-LM9 cells *in vitro*. (A and B): represented pictures of invasion and migration assays after treated by compound **8** in Huh7 cells (magnification × 200, scale bar = 100 μm). The illustration in the upper right corner represented the statistical data of the invasive and migrative Huh 7 cells counted by Image J. (C and D) represented pictures of invasion (magnification × 200, scale bar = 100 μm) and migration (magnification × 200, scale bar = 500 μm) assays after treated by compound **8** in MHCC-LM9 cells. The illustration in the upper right corner represented the statistical data of the invasive and migrative MHCC-LM9 cells counted by Image J. All statistical data are presented as the mean ± SD of three experiments. $^{*}P < 0.05$, $^{***}P < 0.001$ compared with the control group; $^{\#\#}P < 0.01$, $^{\#\#\#}P < 0.001$ compared with the EVO group.

fibrosis. The growth of HCC is dependent on remodeling "stroma", which is comprised of CAFs and extracellular matrix (ECM). Of the two, CAFs play an essential role in the progression, invasion, and chemotherapeutic resistance of HCC. On the other hand, Topo I have been revealed to remarkedly express in many cancer cells, including HCC. Therefore, CAFs and Topo I are two kinds of lucrative targets for novel anti-HCC agents, and the development of novel multi-functional anti-HCC agents taking effect through simultaneously abrogating tumor growth and fibrotic microenvironment is expected to be a promising strategy. In this study, we disclosed 15 evodiamine (EVO) derivatives as Topo I inhibitors for HCC treatment. In comparison with evodiamine, five compounds were proved to possess distinctly anti-proliferation effect *in vitro*. Among them, compound **8** with 10-methyl and N14-phenyl substitution was found to be an effective agent for anti-HCC *in vitro* and displayed lower cytotoxicity to normal hepatic cell than both sorafenib and evodiamine. In subsequent research, compound **8** was verified possessing inhibitory potency on Topo I *in vitro*, which was more potent than that of EVO. Meanwhile, it greatly inhibited the proliferation, significantly alleviated the migration and invasion capacity, induced obvious G_2/M arrest of Huh7 and MHCC-LM9 cells, promoted apoptosis of HCC cells, down-regulated the expression of Col-1 in activated HSC-T6 cells and attenuated the infinitive proliferative capacity and induced-apoptosis of activated HSC cells. Further *in vivo* studies revealed that compound **8** significantly suppressed the growth of xenograft HCC tumors, reduced the weight of GBM tumors (TGI = 40.53%) and displayed low toxicity *in-vivo*. *In vitro* and *in vivo* studies showed that the anti-CAFs and anti-HCC effects of compound **8** were superior to those of EVO. On the basis of these preliminary studies, compound **8** was proved to be an effective anti-HCC agent, which provided a new sight for the development of multi-target anti-HCC agents through simultaneously inhibiting Topo I and CAFs.

4. Experiment

4.1. Chemistry

Proton (^{1}H) and carbon (^{13}C) NMR spectra were respectively recorded on a 400 or 300 MHz spectrometer (Bruker Company, Germany) and a 100 MHz spectrometer. NMR spectra used DMSO-d_6, $CDCl_3$ or $(CD_3)_2CO$-d_6 as solvent (TMS as the internal standard). Carbon chemical shifts are reported relative to a residual solvent peak ($CDCl_3$ at 77.00 ppm, DMSO-d_6 at 39.96 ppm, $(CD_3)_2CO$-d_6 at 29.70 ppm). Proton chemical shifts are reported relative to a residual solvent peak ($CDCl_3$ at 7.26 ppm, DMSO-d_6 at 2.50 ppm, $(CD_3)_2CO$-d_6 at 2.05 ppm). The values of the chemical shifts are expressed in ppm and the coupling constants (*J*) in hertz. The following abbreviations were used to designate multiplicities: s = singlet, d = doublet, t = triplet, q = quartet, quint = quintet, m = multiples, br = broad. High-resolution mass spectrometry (HRMS) was obtained on an Agilent UPLC-IM-QTOF spectrometer (Agilent 6560, USA). Purity of all final compounds was>95% (Agilent 1260 Infinity II; USA).

4.2. HPLC analysis

HPLC analysis was run on an Agilent 1260 Infinity II HPLC chromatogram equipped with an Eclipse Plus C18 column (4.6 × 150 mm, 4 μm) and examined at 254 nm by DAD detector. Mobile phase: 0–7 min, MeOH: H_2O = 20: 80; 7–16 min MeOH: H_2O = 95: 5, 16–25 min MeOH: H_2O = 20: 80. Flow rate is 0.5 mL/min and temperature are maintained at 23 °C.

4.3. General procedure for the preparation of compounds and the characterization data of new compounds

For compounds with oxygen or nitrogen atoms substituted at 14 position, the synthetic procedure is shown as follows: a test tube equipped with a magnetic stir bar was charged with tryptamine (1

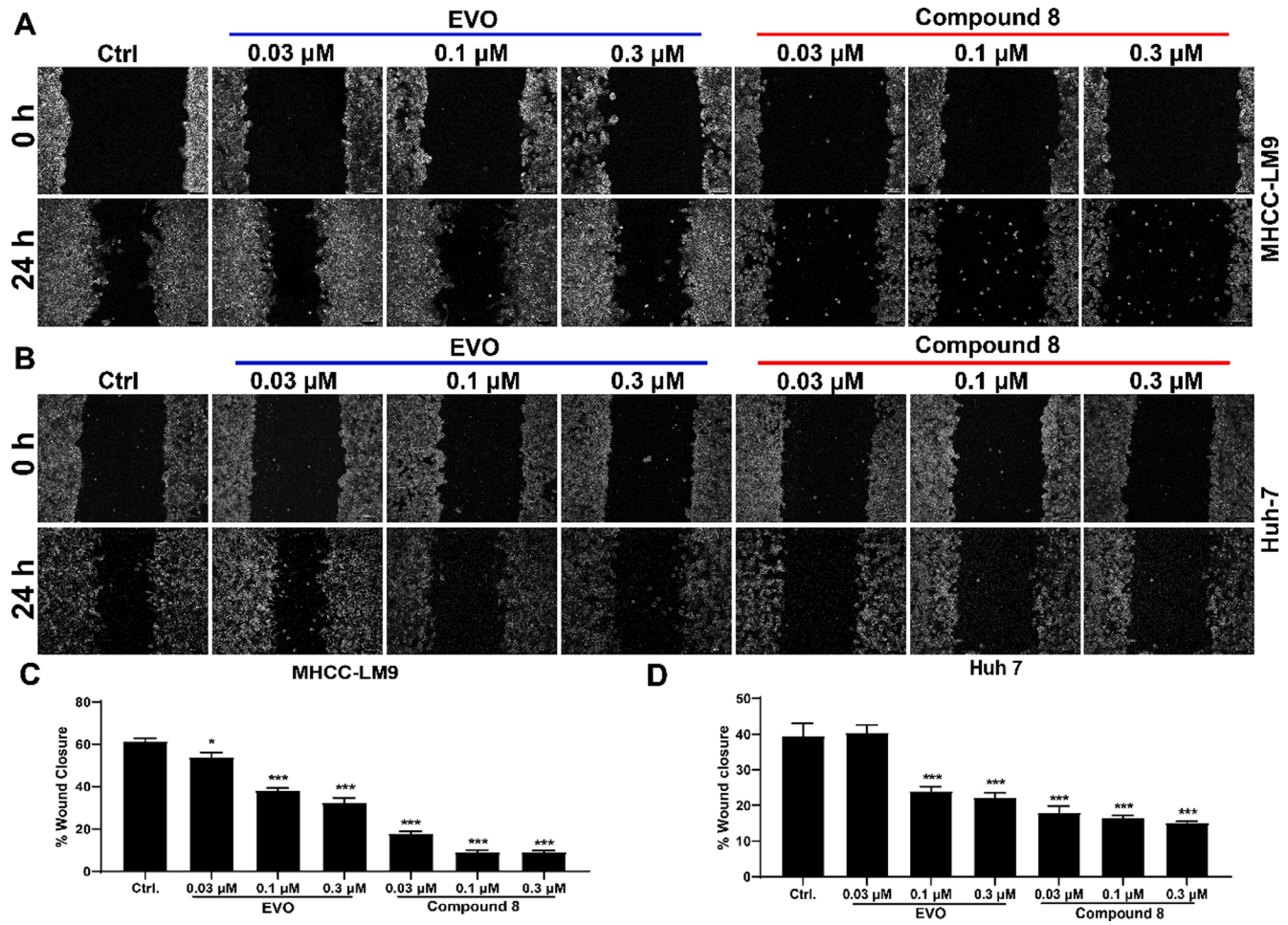

Fig. 7. Compound **8** and EVO decreased the migration rate of MHCC-LM9 and Huh7 cells. Cell monolayers were wounded by scraping with a sterile 200 μL pipette after exposed to compound **8** and EVO for 24 h. Images of horizontal migration of MHCC-LM9 (A) and Huh7 (B) cells at 0 h and 24 h (magnification × 10, scale bar = 100 μm). Analysis of wound closure ratio (C and D). All statistical data are presented as the mean ± SD of three experiments. *P < 0.05; **P < 0.01, ***P < 0.001 compared with the control group.

mmol), 2-(phenylamino) benzoic acid (1 mmol), EDCl (1.2 mmol), HOBt (1.2 mmol), triethylamine (2.5 mmol) and DCM (10 mL). The resulting mixture was stirred for 10 h at room temperature, then added 25 mL of water and 10 mL of saturated brine solution and extracted with DCM for 3 times (3 × 25 mL). The combined organic extracts were concentrated and the resulting residue was purified by column chromatography on silica gel (petroleum ether/ethyl acetate = 3/1) to give intermediates as white solid. For compounds with sulfur atom substituted at 14 position, a test tube equipped with a magnetic stir bar was charged with tryptamine (1.2 mmol), methyl 2-mercaptobenzoate (1 mmol), $AlMe_3$ (1.2 mmol), DCM (10 mL) at 0 °C. The resulting mixture was moved to room temperature and stirred for 12 h, then quenched with HCl (5 M) aqueous solution, and extracted with DCM for 3 times (3 × 25 mL), the combined organic extracts were concentrated and the resulting residue was purified by column chromatography on silica gel (petroleum ether/ethyl acetate = 2/1) to give intermediates as white solid. The next step is that a mixture of the above intermediates (0.1 mmol) was triethyl orthoformate (0.30 mmol), BF_3•Et_2O (0.05 mmol, 0.5 eq) and DMF (1.0 mL) were added and stirred at 100 °C for 5 h under an argon atmosphere. Then, the mixture was added 25 mL of water and 10 mL of saturated brine solution and extracted with ethyl acetate for 3 times (3 × 25 mL). The extract was dried over anhydrous Na_2SO_4 and concentrated under reduced pressure. The crude product was purified by column chromatography (petroleum ether/ ethyl acetate = 4/1) to afford the products as white solid. (compounds **1**–**3** were obtained at 135 °C; compounds **4 – 5** were obtained at room temperature in DCM.)

4.3.1. 14-(pyridin-3-yl)-8,13,13b,14-tetrahydroindolo[2′,3′:3,4]pyrido [2,1-b]quinazolin-5(7H)-one ***(11)***

yellow solid, yield 64%; mp 292.2–294.6 °C.^{1}H NMR (400 MHz, $CDCl_3$) δ 8.44 (s, 1H), 8.36 (s, 1H), 8.33 (s, 1H), 8.14 (d, J = 1.6 Hz, 1H), 8.12 (d, J = 1.6 Hz, 1H), 7.46 (d, J = 7.9 Hz, 1H), 7.43 – 7.32 (m, 3H), 7.24 – 7.08 (m, 4H), 7.01 (dd, J = 8.2, 1.1 Hz, 1H), 4.92 – 4.81 (m, 1H), 3.25 (m, 1H), 2.93 – 2.82 (m, 1H), 2.78 (m, 1H). ^{13}C NMR (100 MHz, $CDCl_3$) δ 164.9, 150.2, 146.6, 146.3, 144.8, 138.6, 136.2, 133.4, 132.2, 129.2, 129.1, 126.6, 124.2, 123.1, 123.0, 121.6, 120.1, 118.9, 114.3, 111.4, 71.9, 42.3, 19.7. MS (ESI^+) *m/z* calcd for $C_{23}H_{19}N_4O^+$ $(M + H)^+$ 367.2, found 367.1. The purity was 96.52% by HPLC analysis.

4.3.2. 14-(6-methylpyridin-3-yl)-8,13,13b,14-tetrahydroindolo [2′,3′:3,4] pyrido [2,1-b] quinazolin-5(7H)-one ***(12)***

yellow solid, yield 58%; mp 261.4–262.8 °C. ^{1}H NMR (400 MHz, $CDCl_3$) δ 8.95 (s, 1H), 8.36 (d, J = 2.7 Hz, 1H), 8.12 (dd, J = 7.9, 1.6 Hz, 1H), 7.46 (d, J = 7.9 Hz, 1H), 7.38 – 7.27 (m, 3H), 7.22 – 7.04 (m, 3H), 6.97 (d, J = 8.4 Hz, 1H), 6.90 (d, J = 8.1 Hz, 1H), 6.31 (s, 1H), 4.86 (m, 1H), 3.24 (m, 1H), 2.94 – 2.74 (m, 2H), 2.42 (s, 3H). ^{13}C NMR (100 MHz, $CDCl_3$) δ 165.0, 155.5, 146.3, 145.6, 139.9, 136.3, 133.3, 133.3, 129.1, 129.0, 126.5, 123.9, 123.4, 123.0, 122.8, 121.5, 119.9, 118.8, 114.0, 111.4, 71.6, 42.0, 23.8, 19.8. MS (ESI^+) *m/z* calcd for $C_{24}H_{21}N_4O^+$ $(M + H)^+$ 381.2, found 381.2. The purity was 95.20% by HPLC analysis.

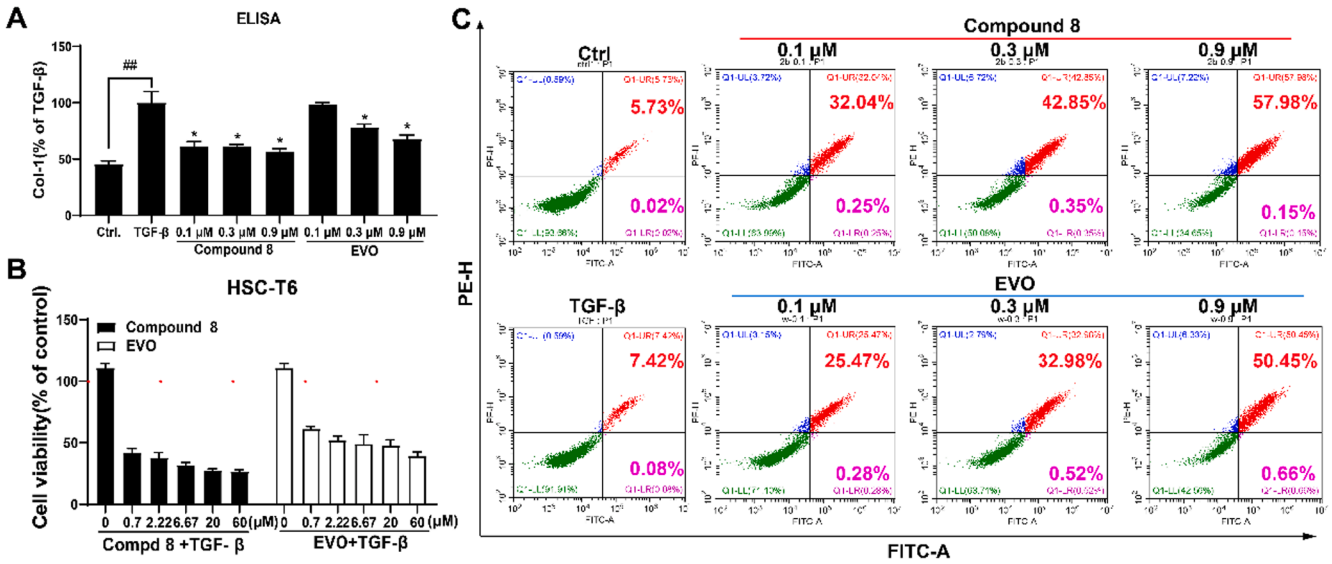

Fig. 8. Compound **8** and EVO suppressed TGF-β-induced the activation of HSC-T6 cells and their effects on antiproliferation and induced-apoptosis of activated HSC-T6 cells in 24 h. HSC-T6 cells were exposed to compound **8** at different concentrations for 24 h in the presence of TGF-β (10 ng/mL). Col-1 as a biomarker protein expressed by activated HSC-T6 cells was measured by ELISA assay(A). HSC-T6 cells were stimulated by TGF-β (10 ng/mL) for 24 h before compound **8** at different concentrations were added into each well and incubated for 24 h, except for the control well. CCK-8 assay was first performed to evaluate antiproliferation of compound **8** and EVO on TGF-β-induced activation of HSC-T6 cell. (B): the cell viability of compounds at the indicated concentrations (0.70, 2.22, 6.67, 20 and 60 μM). (C): Apoptosis analysis of activated HSC-T6 cells by flow cytometry using Annexin V/PI double staining. All statistical data are presented as the mean ± SD of three experiments. *P < 0.05; **P < 0.01, ***P < 0.001 compared with the TGF-β group; $^{\#\#}$P < 0.01, $^{\#\#\#}$P < 0.001 compared with the control group.

4.3.3. 14-(6-chloropyridin-3-yl)-8,13,13b,14-tetrahydroindolo [2′,3′:3,4] pyrido[2,1-b]quinazolin-5(7H)-one ***(13)***

yellow solid, yield 66%; mp 277.4–278.1 °C. ^{1}H NMR (400 MHz, $CDCl_3$) δ 8.83 (s, 1H), 8.15 (dd, *J* = 7.9, 1.6 Hz, 1H), 8.10 – 7.98 (d, 1H), 7.48 – 7.44 (d, 1H), 7.40 (m, 1H), 7.35 (d, *J* = 8.3, 0.9 Hz, 1H), 7.25 – 7.17 (m, 3H), 7.15 – 7.06 (m, 2H), 6.97 (d, *J* = 8.2, 1.1 Hz, 1H), 6.30 (s, *J* = 1.5 Hz, 1H), 4.82 (m, 1H), 3.22 (m, 1H), 2.85 – 2.66 (m, 2H). ^{13}C NMR (100 MHz, $CDCl_3$) δ 164.8, 147.5, 146.6, 145.2, 141.2, 136.4, 135.6, 133.5, 129.2, 127.9, 126.3, 124.8, 124.2, 123.7, 123.3, 122.1, 120.1, 118.9, 114.5, 111.5, 71.3, 41.7, 19.8. MS (ESI^+) *m/z* calcd for $C_{23}H_{18}ClN_4O^+$ $(M + H)^+$ 401.1, found 401.1. The purity was 95.60% by HPLC analysis.

4.3.4. 14-(5-bromopyridin-3-yl)-8,13,13b,14-tetrahydroindolo[2′,3′:3,4] pyrido[2,1-b]quinazolin-5(7H)-one ***(14)***

yellow solid, yield 71%; mp 282.5–283.1 °C. ^{1}H NMR (400 MHz, $CDCl_3$) δ 8.44 (s, 1H), 8.36 (d, *J* = 2.0 Hz, 1H), 8.29 (d, *J* = 2.3 Hz, 1H), 8.14 (dd, *J* = 7.9, 1.6 Hz, 1H), 7.49 – 7.41 (m, 3H), 7.36 (d, *J* = 8.3, 1.0 Hz, 1H), 7.22 (m, 2H), 7.12 (m, 1H), 7.04 (d, *J* = 8.2, 1.1 Hz, 1H), 6.35 (s, *J* = 1.6 Hz, 1H), 4.86 (m, 1H), 3.25 (m, 1H), 2.95 – 2.71 (m, 2H). ^{13}C NMR (100 MHz, $CDCl_3$) δ 164.7, 147.1, 144.2, 144.0, 143.5, 137.0, 136.2, 134.3, 133.6, 132.1, 129.4, 128.6, 126.6, 125.0, 123.4, 121.88, 120.3, 119.0, 114.6, 111.4, 72.0, 42.3, 19.8. MS (ESI^+) *m/z* calcd for $C_{23}H_{18}BrN_4O^+$ $(M + H)^+$ 445.1, found 445.0. The purity was 96.74% by HPLC analysis.

4.3.5. 14-(quinoxalin-6-yl)-8,13,13b,14-tetrahydroindolo[2′,3′:3,4] pyrido[2,1-b]quinazolin-5(7H)-one ***(15)***

yellow solid, yield 66%; mp 315.2–316.6 °C. 1H NMR (400 MHz, $CDCl_3$) δ 8.86 (s, 1H), 8.76 – 8.69 (m, 2H), 8.07 (dd, *J* = 8.1, 1.7 Hz, 1H), 7.99 (d, *J* = 9.1 Hz, 1H), 7.84 (d, *J* = 2.5 Hz, 1H), 7.70 (dd, *J* = 9.1, 2.6 Hz, 1H), 7.45 (d, *J* = 7.9 Hz, 1H), 7.35 (td, *J* = 7.7, 1.6 Hz, 1H), 7.28 (d, *J* = 8.6 Hz, 1H), 7.19 – 7.06 (m, 4H), 6.56 (s, 1H), 4.89 (dd, *J* = 12.9, 5.4 Hz, 1H), 3.30 – 3.06 (m, 2H), 2.68 (dd, *J* = 15.4, 4.4 Hz, 1H).13C NMR (100 MHz, $CDCl_3$) δ 164.7, 148.0, 145.4, 144.0, 143.7, 142.4, 140.4, 136.0, 133.3, 130.8, 130.4, 129.3, 127.1, 126.1, 124.0, 122.9, 121.8, 120.5, 120.0, 119.4, 118.7, 113.7, 111.4, 73.3, 43.8, 19.6. MS (ESI^+) *m/z* calcd for $C_{26}H_{20}N_5O^+$ $(M + H)^+$ 418.2, found 418.1. The purity was 97.03% by HPLC analysis.

4.4. Cell lines and culture

HL-7702, HepG2, MHCC-LM9, Huh7 cell lines were purchased from Institute of Biochemistry and Cell Biology of the Chinese Academy of Sciences (Shanghai, China). All cell lines were cultivated in a humidified environment containing 95% air and 5% CO_2 at 37 °C, grown in DMEM media supplemented with 10% FBS (fetal bovine serum, Gemini Foundational), 100 U/mL penicillin and 100 μg/mL streptomycin.

4.5. Cell viability assay

MHCC-LM9, Huh7, HL-7702 and HepG2 (2–5 × 10^3 cells/well) cells were separately plated into 96-well microplates and cultured 24 h. The cellular viability was assessed using a Cell Counting Kit-8 kit (Meilunbio, MA0218-5-Apr-01F), after cells were treated with target compounds at the concentration 0, 0.156, 0.625, 2.5, 10, 40 μM for 48 h. The absorbance value (OD) was measured using a microplate reader (TECAN, spark, Switzerland) at 450 nm. The IC_{50} values were calculated by inhibitory curves using SPSS. All assays were in triplicate and represented in mean ± SD values.

4.6. Enzyme inhibition assay

EVO, CPT, VP16 and compound **8** were dissolved in DMSO and were examined at final concentrations of 100, 50, 10 in Topo I inhibition assay (TaKaRa Biotechnology). The Topo I reaction mixture contained Topo I (0.5 units, 0.5 μL), tested compounds (0.2 μL), buffer (pH 8.0 35 mM Tris-HCl, 72 mM KCl, 5 mM $MgCl_2$, 5 μM dithiothreitol, 5 mM spermidine, 2 μL), 0.1% bovine serum albumin (BSA, 2 μL), pBR322 plasmid DNA (0.125 μg, 0.5 μL), and distilled water in a final volume of 20 μL. Reactions were incubated for 30 min at 37 °C. All the reactions were vortexed for 10 s and centrifuged for 2 min. Then, 6 μL of 6 × gel loading buffer (0.25% bromophenol blue and 50% glycerol) was added. Products were analyzed by gel electrophoresis in a 0.8% agarose gel

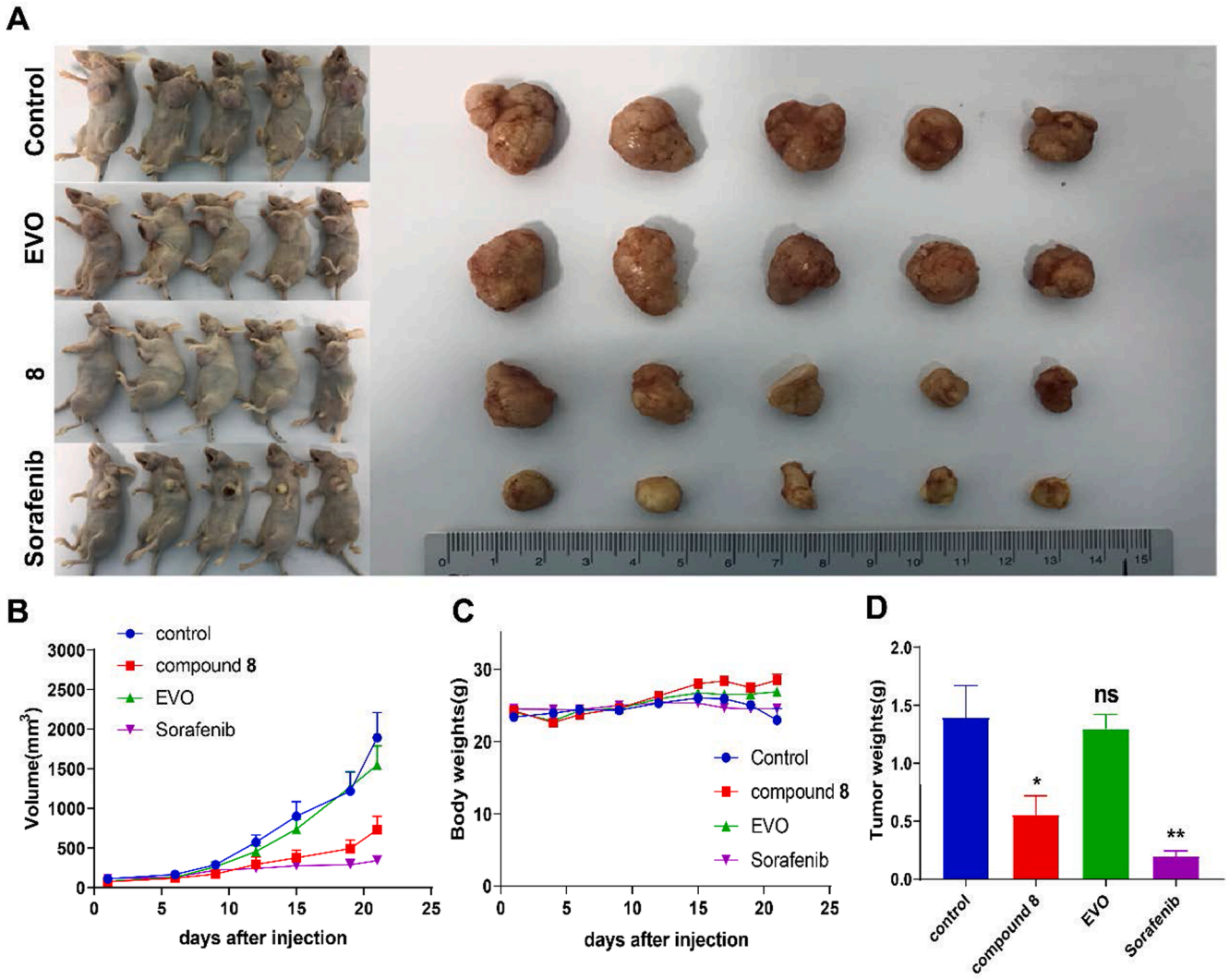

Fig. 9. Compound **8** inhibited tumor growth in the xenograft nude mice model. (A) Pictures of nude mice and separated entire MHCC-LM9 tumor tissue. (B) Growth curve of implanted MHCC-LM9 xenograft in nude mice measured by volume. (C) The body weight change of nude mice treated with different compounds. (D) The tumor weight of each group. Data are presented as the mean ± SEM (n = 5); *P < 0.05; **P < 0.01, ns: no significant, compared with the control group.

without EtBr. To visualize the DNA band, soaking the gel in EtBr work solution (0.5 μg/mL) for 30 min after DNA electrophoresis. The DNA bands were visualized under UV light.

4.7. EdU assay

MHCC-LM9, and Huh7 cells were seeded at a density of 1×10^3 cells/well onto 96-well plates and incubated until the cells attached, then treated with different various of compound **8** and EVO at the final concentrations of 0.1, 0.3, and 0.9 μM. EdU assay was performed according to the manufacturer's instructions (Cat.#: C10310-1, Ribobio,) after treatment for 24 h. In short, containing 50 μM/100 μL of EdU DMEM was added and cultured for another 2 h. Removing the medium before cells were washed with PBS three times. And then, 4% paraformaldehyde was added into each well to fix cells at room temperature for 30 min. 0.5% TritonX-100 solution was added after adding 50 μL of 2 mg/mL glycine and incubated min on shaker for 5 min, following by washed away with PBS. Cells were stained with Apollo in the dark for 30 min. Subsequently, staining with Hoechst 33,342 (Solarbio, Cat.#: B8030) for 5 min in the dark, cells were observed by a fluorescence microscope (Moticam Pro 282B, China).

4.8. Colony formation assay

Huh7 (1×10^3 cells/well), and MHCC-LM9 (1×10^3 cells/well) cells were seeded onto 6-well plates and cultured 24 h. After being incubated with tested compounds at indicated concentrations (0.1, 0.3 ,0.9 μM) for 7 days, changed medium every 3 days, cells were fixed with methanol and stained with 1% crystal violet. Colonies of ≥ 50 cells were counted under microscope at 4 × lens.

4.9. Cell cycle analysis

MHCC-LM9 ($2–5 \times 10^4$ cells/well), and Huh7 ($2–5 \times 10^4$cells/well) cells were separately seeded into 6-well microplates and cultured 24 h and then co-cultured with compound **8** and EVO at indicated concentrations (0.1, 0.3, and 0.9 μM) for 24 h. Then the cells were harvested and fixed with 70% pre-cooled ethanol at 4 °C for overnight. After removing ethanol by centrifugation, the fixed cells were resuspended in PBS and treated with RNase A followed by staining with PI for 10 min. The cell cycle analysis was determined by Flow cytometry (Becton Dickinson, USA). Data were analyzed by Modfit software.

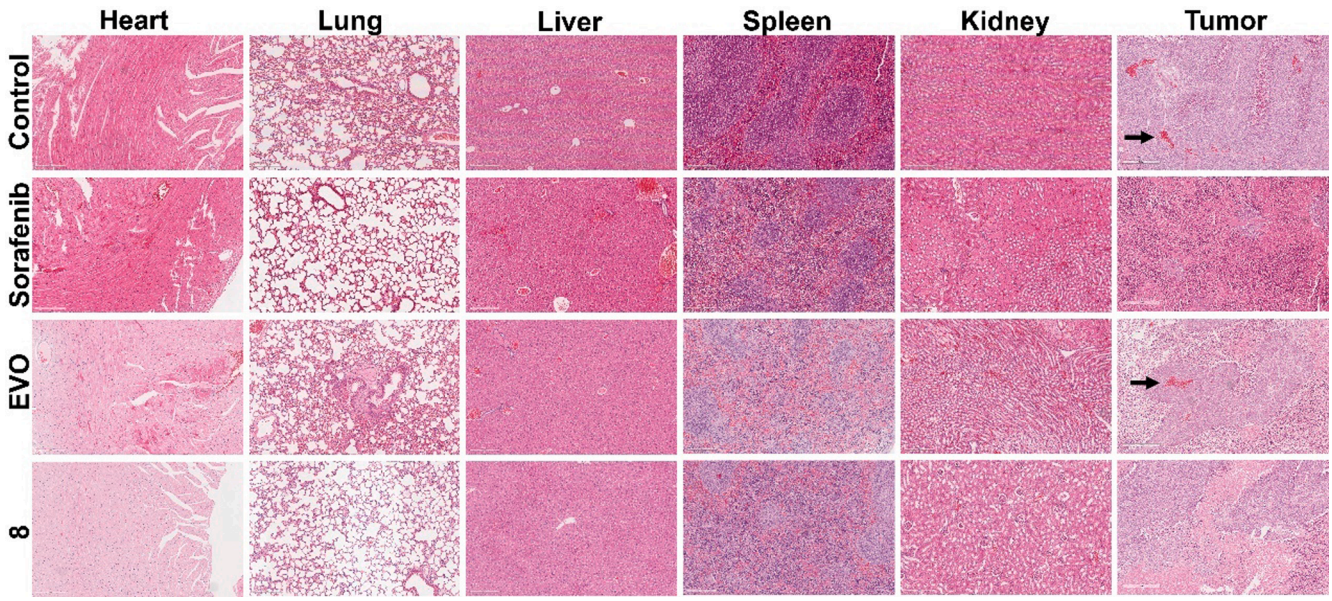

Fig. 10. Histopathological images of mice tissues (heart, lung, liver, spleen, kidney and tumor, magnification × 100, scale bar = 300 μm), The black arrow marked vessels in the tumor.

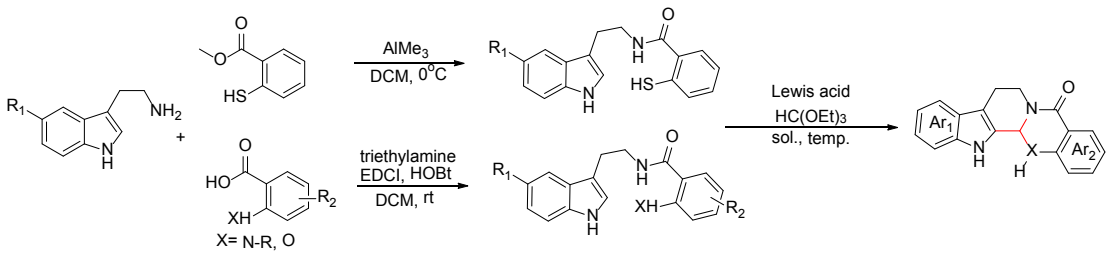

4.10. Cell apoptosis and Giemsa staining assays

Huh7 (2–5 × 10^4 cells/mL) cells were seeded into 6-well plates and incubated until the cell attached, then treated with tested compounds at 0.1, 0.3 and 0.9 μM for 48 h. After that, the cells were collected by trypsinization, washed with PBS twice, and stained with PI and FITC-Annexin-V for 0.5 h in the dark. Then, the flow cytometry (BD Bioscience, USA) was used for determined the percentages of apoptotic cells. Data were analyzed by Flow J software. Huh7 cells at the density of 2–5 × 10^4 were plated into 6-well plates and incubated for 24 h. Cells were treated with evo and compound **8** at the concentrations of 0.1, 0.3 and 0.9 μM. After cultured for 48 h, removed medium and cells were washed with PBS and fixed with 4% paraformaldehyde for 3 min. Next, cells were stained with Giemsa reagent (Solarbio, Cat. #: G1010) for 30 min. The reagent was rinsed away with water and observed under inverted microscope.

4.11. Cell invasion and migration assays

The *vitro* cell invasion and migration assays were employed using the upper chamber with or without Matrigel (BD) of a 24-well Transwell plate (Costar, Cambridge, MA). Huh7 and MHCC-LM9 cells suspended with FBS-free medium at a density of 5 × 10^4/mL were added into the upper chamber and the outer chamber contained 700 μL medium (15% FBS). At the same time, the various concentrations of compound **8** (0.1, 0.3 and 0.9 μM) and EVO (0.9 μM) were added into the chambers and incubated at 37℃ for 24 h. Next, cells in upper chamber were removed with cotton swabs. Invaded and migrated cells on the outer surface of the chamber, were fixed with 4% paraformaldehyde for 3 min and stained with crystal violet (0.1%). Five random views were chosen for cell counting (magnification × 200).

4.12. Scratch assay

MHCC-LM9 and Huh7 cells were cultured in 6 well plates to 90% confluence in DMEM supplemented with 10% FBS. Cell monolayers were wounded by scraping with a sterile 200 μL pipet tip. The cells were removed the medium and washed with PBS three times before treated with EVO and compound **8** at the concentrations of 0.03, 0.1 and 0.3 μM. After cultured for 24 h. Images were captured of each scratch at time points 0 h and 24 h. Measurements were taken from edge to edge at time 0 h and compared to measurements from 24 h using ImageJ software.

4.13. The activation of HSC-T6 cells stimulated by TGF-β

HSC-T6 (2–5 × 10^3 cells/mL) cells were seeded into 96-well microplate at 37℃, 5% CO_2 for overnight, and then were treated with TGF-β (10 ng/mL) for 24 h, equal volume of water was added into control well. Next, TGF-β induced cells exposed to various concentrations (0, 0.7, 2.2, 6.6, 20, 60 μM) of tested compound. After incubating for 24 h, the cellular viability was measured by CCK-8 method. The absorbance value (OD) was tested using a microplate reader (TECAN, spark, Switzerland) at 450 nm. the cellular viability was calculated using the following equation: $[(OD_{Control}\text{-}OD_{Blank})/(OD_{Control}\text{-}OD_{Blank})] \times 100\%$. All assays were in triplicate and represented in mean ± SD values. HSC-T6 cells were exposed to compound **8** at different concentrations for 24 h in the

presence of TGF-β (10 ng/mL). At the same time, equal volume of DMSO was added into TGF-β treated well and control group without TGF-β. Cells were collected after washing with PBS, were lysed by freeze–thaw cycles three time, followed by centrifugation at 5000 rpm at 4 °C for 15 min. The protein concentrations were determined by BCA kit (Beyotime, China), adjusted by PBS to the same concentration. Samples was added in ELISA microplates precoated with polyclonal Col-1 antibodies (shanghai mlbio, China), incubated for 45 min at 37 °C. After washed with ELISA Wash buffer five times, Horseradish Peroxidase (HRP) solution was added into to each microplate well and incubated for 30 min. Subsequently, Solution A and solution B added into each well before washed with ELISA Wash buffer five times, incubated for 15 min at 37 °C, terminated the reaction by adding the Stop solution and the absorbance value (OD) was measured by a microplate reader at 450 ± 2 nm. The sample OD value is interpolated onto formula for the standard curve to determine their content of Col-1. The results were calculated from at least three independent experiments. HSC-T6 (2–5 × 10^4 cells/mL) cells were seeded into 6-well plates at 37 °C, 5% CO_2 for overnight, and then were treated with TGF-β (10 ng/mL) for 24 h. TGF-β induced cells exposed to various concentrations (0, 0.1 0.3 and 0.9 μM) of tested compound. After incubating for 24 h, apoptosis analysis was measured by flow cytometry using Annexin V/PI double staining. All statistical data are presented as the mean ± SD of three experiments. *P < 0.05; **P < 0.01, ***P < 0.001 compared with the TGF-β group; $^{\#\#}$P < 0.01, $^{\#\#\#}$P < 0.001 compared with the control group.

4.14. In vivo antitumor Activity

The *in vivo* antitumor activities of compound **8** and evodiamine at a single dose of 50 mg/kg and Sorafenib at a single dose of 10 mg/kg were evaluated. Nude male mice (certificate SCXK-2007–0005, weighing 18–20 g) were obtained from BEIJING HFK BIOSCIENCE CO., LTD. Suspensions of MHCC-LM9 cells were implanted subcutaneously into the right axilla region of the mice. Treatment began when the implanted tumors reached a volume of approximately 100 mm^3 (after 10 days). The animals were randomized into the four groups (five animals/group), and in the tenth day, the treatments were administered by intraperitoneal injection. twice per day for 21 consecutive days. Observations were made for 21 days after the first injection. Tumor volumes were calculated by length × $width^2$ × 0.50 using radial measurements performed with calipers. Tumor volumes and body weights were monitored every 2 days over the course of treatment. Mice were sacrificed on day 31 after implantation of the cells, and tumors were removed and weighed. Afterward, whole tumors were fixed in 4% paraformaldehyde at 4 °C for more than 24 h and pathological observed by hematoxylin and eosin staining. The pathological images were recorded by microscope (Motic, China). Fresh blood is collected for the detection of blood routine and biochemistry. The *vivo* study was performed according to the Institutional Animal Care and Use Committee (IACUC) guidelines and was approved by the Institutional Animal Ethics Committee of Lanzhou University.

4.15. Statistical analysis

All results were showed as the mean ± SD/SEM, significance between the groups was determined by analysis of variance (ANOVA), followed by Fisher's PLSD procedure for post hoc comparison. The data were analyzed by SPSS 25.0 software, P values of<0.05 were considered significant.

Declaration of Competing Interest

The authors declare that they have no known competing financial interests or personal relationships that could have appeared to influence the work reported in this paper.

Acknowledgements

We thank Dr. Na Yan for HRMS analysis (UPLC-IM-QTOF, 6560, ion source: ESI or APCI). This work was technically supported by University of South China, Lanzhou University, and Gansu Provincial Hospital. This work was financially supported by the Gansu Province Science Foundation for Distinguished Young Scholars (20JR5RA304) and Recruitment Program of Global Experts (1000 Talents Plan). Dr. Xiangyong Hao thanks the financially support from the Gansu Province Youth Innovative Talents Project (2021, Xiangyong Hao), Health Industry Scientific Research Program of Gansu Province (GSWSKY2020-06), the Natural Science Foundation for Young Scientists and the Science & Technology Planning Project of Gansu Province (18JR3RA058), and Research Projects of Gansu Provincial Hospital (Grant No.: 19SYPYB-7, 18GSSY3-1).

Appendix A. Supplementary material

Supplementary data to this article can be found online at https://doi.org/10.1016/j.bioorg.2021.105154.

References

[1] F. Bray, J. Ferlay, I. Soerjomataram, R.L. Siegel, L.A. Torre, A. Jemal, Global cancer statistics 2018: GLOBOCAN estimates of incidence and mortality worldwide for 36 cancers in 185 countries, CA Cancer J. Clin. 68 (6) (2018) 394–424.
[2] A. Forner, M. Gilabert, J. Bruix, J.L. Raoul, Treatment of intermediate-stage hepatocellular carcinoma, Nat. Rev. Clin. Oncol. 11 (9) (2014) 525–535.
[3] C.E.J.A.L.-B.P.A. Bonilla-Reyes, Immune checkpoint inhibitors for hepatocellular carcinoma, Hepat. Oncol. 3 (3) (2016) 201–211.
[4] J. Guo, L. Li, B. Guo, D. Liu, J. Shi, C. Wu, J. Chen, X. Zhang, J. Wu, Mechanisms of resistance to chemotherapy and radiotherapy in hepatocellular carcinoma, Translational Cancer Res. 7 (3) (2018) 765–781.
[5] N. Dong, X. Shi, S. Wang, Y. Gao, Z. Kuang, Q. Xie, Y. Li, H. Deng, Y. Wu, M. Li, J. L. Li, M2 macrophages mediate sorafenib resistance by secreting HGF in a feed-forward manner in hepatocellular carcinoma, Br. J. Cancer 121 (1) (2019) 22–33.
[6] M. Bouattour, N. Mehta, A.R. He, E.I. Cohen, J.C. Nault, Systemic Treatment for Advanced Hepatocellular Carcinoma, Liver Cancer 8 (5) (2019) 341–358.
[7] S. Ogasawara, Y. Ooka, N. Itokawa, M. Inoue, S. Okabe, A. Seki, Y. Haga, M. Obu, M. Atsukawa, E. Itobayashi, H. Mizumoto, N. Sugiura, R. Azemoto, K. Kanayama, H. Kanzaki, S. Maruta, T. Maeda, Y. Kusakabe, M. Yokoyama, K. Kobayashi, S. Kiyono, M. Nakamura, T. Saito, E. Suzuki, S. Nakamoto, S. Yasui, A. Tawada, T. Chiba, M. Arai, T. Kanda, H. Maruyama, N. Kato, Sequential therapy with sorafenib and regorafenib for advanced hepatocellular carcinoma: a multicenter retrospective study in Japan, Invest. New Drugs 38 (1) (2020) 172–180.
[8] C. Molinaro, A. Martoriati, L. Pelinski, K. Cailliau, Copper Complexes as Anticancer Agents Targeting Topoisomerases I and II, Cancers (Basel) 12 (10) (2020) 2863.
[9] J.M. Llovet, R.K. Kelley, A. Villanueva, A.G. Singal, E. Pikarsky, S. Roayaie, R. Lencioni, K. Koike, J. Zucman-Rossi, R.S. Finn, Hepatocellular carcinoma, Nat. Rev. Dis. Primers 7 (1) (2021) 6.
[10] V. Hernandez-Gea, S. Toffanin, S.L. Friedman, J.M. Llovet, Role of the microenvironment in the pathogenesis and treatment of hepatocellular carcinoma, Gastroenterology 144 (3) (2013) 512–527.
[11] L. Kaps, D. Schuppan, Targeting Cancer Associated Fibroblasts in Liver Fibrosis and Liver Cancer Using Nanocarriers, Cells 9 (9) (2020) 2027.
[12] Y. Myojin, H. Hikita, M. Sugiyama, Y. Sasaki, K. Fukumoto, S. Sakane, Y. Makino, N. Takemura, R. Yamada, M. Shigekawa, T. Kodama, R. Sakamori, S. Kobayashi, T. Tatsumi, H. Suemizu, H. Eguchi, N. Kokudo, M. Mizokami, T. Takehara, Hepatic Stellate Cells in Hepatocellular Carcinoma Promote Tumor Growth Via Growth Differentiation Factor 15 Production, Gastroenterology 160 (2021) 1741–1754.
[13] Y. Sun, L. Wu, Y. Zhong, K. Zhou, Y. Hou, Z. Wang, Z. Zhang, J. Xie, C. Wang, D. Chen, Y. Huang, X. Wei, Y. Shi, Z. Zhao, Y. Li, Z. Guo, Q. Yu, L. Xu, G. Volpe, S. Qiu, J. Zhou, C. Ward, H. Sun, Y. Yin, X. Xu, X. Wang, M.A. Esteban, H. Yang, J. Wang, M. Dean, Y. Zhang, S. Liu, X. Yang, J. Fan, Single-cell landscape of the ecosystem in early-relapse hepatocellular carcinoma, Cell 184 (2) (2021) 404–421 e16.
[14] H. Wu, H. Xing, M.C. Wu, F. Shen, Y. Chen, T. Yang, Extracellular-vesicles delivered tumor-specific sequential nanocatalysts can be used for MRI-informed nanocatalytic Therapy of hepatocellular carcinoma, Theranostics 11 (1) (2021) 64–78.
[15] M.S. Butler, A.A. Robertson, M.A. Cooper, Natural product and natural product derived drugs in clinical trials, Nat. Prod. Rep. 31 (11) (2014) 1612–1661.
[16] Y. Huang, S. Chen, S. Wu, G. Dong, C. Sheng, Evodiamine-inspired dual inhibitors of histone deacetylase 1 (HDAC1) and topoisomerase 2 (TOP2) with potent antitumor activity, Acta Pharm. Sin B 10 (7) (2020) 1294–1308.
[17] G. Dong, C. Sheng, S. Wang, Z. Miao, J. Yao, W. Zhang, Selection of evodiamine as a novel topoisomerase I inhibitor by structure-based virtual screening and hit optimization of evodiamine derivatives as antitumor agents, J. Med. Chem. 53 (21) (2010) 7521–7531.

[18] W. Yang, X. Gong, X. Wang, C. Huang, A mediator of phosphorylated Smad2/3, evodiamine, in the reversion of TAF-induced EMT in normal colonic epithelial cells, Invest. New Drugs 37 (5) (2019) 865–875.
[19] D. Yang, L. Li, S. Qian, L. Liu, Evodiamine ameliorates liver fibrosis in rats via TGF-beta1/Smad signaling pathway, J. Nat. Med. 72 (1) (2018) 145–154.
[20] X. Li, J. Ge, Q. Zheng, J. Zhang, R. Sun, R. Liu, Evodiamine and rutaecarpine from Tetradium ruticarpum in the treatment of liver diseases, Phytomedicine 68 (2020), 153180.
[21] S.-Y. Liang, Y.-C. Zeng, Q.-Q. Jiang, J.-H. Wu, Z.-Z. Wu, Pharmacokinetic studies of multi-bioactive components in rat plasma after oral administration of Xintiantai I extract and effects of guide drug borneol on pharmacokinetics, Chinese Herbal Med. 12 (1) (2020) 79–87.
[22] Z. Zhang, T. Fang, H. Zhou, J. Yuan, Q. Liu, Characterization of the in Vitro Metabolic Profile of Evodiamine in Human Liver Microsomes and Hepatocytes by UHPLC-Q Exactive Mass Spectrometer, Front. Pharmacol. 9 (2018) 130.
[23] M.-H. Shyr, L.-C. Lin, T.-Y. Lin, T.-H. Tsai, Determination and pharmacokinetics of evodiamine in the plasma and feces of conscious rats, Anal. Chim. Acta 558 (1–2) (2006) 16–21.
[24] J. Yuan, Y. Wang, R. An, S. Wang, S.J. Li, J.Y. Jia, S.W. Bligh, X.H. Wang, Y.M. Ma, Simultaneous determination of six alkaloids and one monoterpene in rat plasma by liquid chromatography-tandem mass spectrometry and pharmacokinetic study after oral administration of a Chinese medicine Wuji Pill, J. Chromatogr. B Analyt. Technol. Biomed. Life Sci. 895–896 (2012) 154–161.
[25] L. Wang, K. Fang, J. Cheng, Y. Li, Y. Huang, S. Chen, G. Dong, S. Wu, C. Sheng, Scaffold Hopping of Natural Product Evodiamine: Discovery of a Novel Antitumor Scaffold with Excellent Potency against Colon Cancer, J. Med. Chem. 63 (2) (2020) 696–713.
[26] X. Hu, R. Jiao, H. Li, X. Wang, H. Lyu, X. Gao, F. Xu, Z. Li, H. Hua, D. Li, Antiproliferative hydrogen sulfide releasing evodiamine derivatives and their apoptosis inducing properties, Eur. J. Med. Chem. 151 (2018) 376–388.
[27] S. Wang, K. Fang, G. Dong, S. Chen, N. Liu, Z. Miao, J. Yao, J. Li, W. Zhang, C. Sheng, Scaffold Diversity Inspired by the Natural Product Evodiamine: Discovery of Highly Potent and Multitargeting Antitumor Agents, J. Med. Chem. 58 (16) (2015) 6678–6696.
[28] G. Dong, S. Wang, Z. Miao, J. Yao, Y. Zhang, Z. Guo, W. Zhang, C. Sheng, New tricks for an old natural product: discovery of highly potent evodiamine derivatives as novel antitumor agents by systemic structure-activity relationship analysis and biological evaluations, J. Med. Chem. 55 (17) (2012) 7593–7613.
[29] X. Liang, Q. Wu, S. Luan, Z. Yin, C. He, L. Yin, Y. Zou, Z. Yuan, L. Li, X. Song, M. He, C. Lv, W. Zhang, A comprehensive review of topoisomerase inhibitors as anticancer agents in the past decade, Eur. J. Med. Chem. 171 (2019) 129–168.
[30] T. Zhang, Z. Lai, S. Yuan, Y.Y. Huang, G. Dong, C. Sheng, H. Ke, H.B. Luo, Discovery of Evodiamine Derivatives as Highly Selective PDE5 Inhibitors Targeting a Unique Allosteric Pocket, J. Med. Chem. 63 (17) (2020) 9828–9837.
[31] J.X. Yingjie Zhang, Yuankun Zhang, Lu Jia and Guanghui Liu, New tricks for an old dog: discovery, synthesis, in vitro and in vivo antitumor evaluation as well as docking studies of novel rutaecarpine derivatives as Topoisomerase I inhibitors, J. Chem. Pharm. Res. 7 (4) (2015) 93–102.
[32] J.D. Deng, S. Lei, Y. Jiang, H.H. Zhang, X.L. Hu, H.X. Wen, W. Tan, Z. Wang, A concise synthesis and biological study of evodiamine and its analogues, Chem. Commun. (Camb.) 55 (21) (2019) 3089–3092.
[33] D. Jing, C. Lu, Z. Chen, S. Jin, L. Xie, Z. Meng, Z. Su, K. Zheng, Light-Driven Intramolecular C-N Cross-Coupling via a Long-Lived Photoactive Photoisomer Complex, Angew. Chem. Int. Ed. Engl. 58 (41) (2019) 14666–14672.
[34] L. Zhu, J. Li, X. Fan, X. Hu, J. Chen, Y. Liu, X. Hao, T. Shi, Z. Wang, Q. Zhao, Design, synthesis and antitumor activity evaluation of Chrysamide B derivatives, Bioorg. Chem. 111 (2021), 104828.
[35] H. Cai, B. Shao, Y. Zhou, Z. Chen, High expression of TOP2A in hepatocellular carcinoma is associated with disease progression and poor prognosis, Oncol. Lett. 20 (5) (2020) 232.
[36] L. Shi, F. Yang, F. Luo, Y. Liu, F. Zhang, M. Zou, Q. Liu, Evodiamine exerts anti-tumor effects against hepatocellular carcinoma through inhibiting beta-catenin-mediated angiogenesis, Tumour Biol. 37 (9) (2016) 12791–12803.
[37] L. Kaps, D. Schuppan, Targeting Cancer Associated Fibroblasts in Liver Fibrosis and Liver Cancer Using Nanocarriers, Cells 9 (9) (2020).
[38] R.L. Barrett, E. Pure, Cancer-associated fibroblasts and their influence on tumor immunity and immunotherapy, Elife 9 (2020) 57243.
[39] J. Baglieri, D.A. Brenner, T. Kisseleva, The Role of Fibrosis and Liver-Associated Fibroblasts in the Pathogenesis of Hepatocellular Carcinoma, Int. J. Mol. Sci. 20 (7) (2019).
[40] C. Jia, G. Wang, T. Wang, B. Fu, Y. Zhang, L. Huang, Y. Deng, G. Chen, X. Wu, J. Chen, Y. Pan, Y. Tai, J. Liang, X. Li, K. Hu, B. Xie, S. Li, Y. Yang, G. Chen, Q. Zhang, W. Liu, Cancer-associated Fibroblasts induce epithelial-mesenchymal transition via the Transglutaminase 2-dependent IL-6/IL6R/STAT3 axis in Hepatocellular Carcinoma, Int. J. Biol. Sci. 16 (14) (2020) 2542–2558.